

## Supplementary file

for

### Oriented generation of singlet oxygen in H<sub>2</sub>O<sub>2</sub> activation for water

### decontamination: Regulation of oxygen vacancy over $\alpha$ -MnO<sub>2</sub> nanocatalyst

Xixi Chen<sup>a</sup>, Yanjun Li<sup>a</sup>, Wanyi Fu<sup>b, \*</sup>, Shuanghong Tian<sup>c</sup>, Yulong Yang<sup>a</sup>, Kai Yang<sup>c</sup>, Xuanbo Xu<sup>c</sup>,

Xihui Zhang<sup>a, \*</sup>

<sup>a</sup> Institute of Environment and Ecology, Tsinghua Shenzhen International Graduate School, Tsinghua University, Shenzhen, 518055, China

<sup>b</sup> State Key Laboratory of Pollution Control and Resource Reuse, School of Environment, Nanjing University, Nanjing, 210023, China

<sup>c</sup> Guangdong Provincial Key Laboratory of Environmental Pollution Control and Remediation, School of Environmental Science & Engineering, Sun Yat-sen University, Guangzhou 510275, P. R. China

<sup>d</sup> Guangdong Guangye Equipment Manufacturing Group Co. LTD, Guangzhou, 510275, China

\* Corresponding authors. E-mail address: fu.wanyi@nju.edu.cn (W. Fu); xihuizh@tsinghua.edu.cn (X. Zhang)

## Contents

**Text S1.** Quantitative detection of  $^1\text{O}_2$ .

**Text S2.** Density functional theory (DFT) calculation.

**Table S1.** Parameters of pharmaceutical wastewater.

**Table S2.** Detected emerging organic contaminants in the pharmaceutical wastewater.

**Fig. S1.** Adsorption of OTC by different  $\text{MnO}_2$  catalysts under various pH conditions. Conditions:

[catalysts] = 300 mg/L, [OTC] = 5 mg/L, pH = 4.0–11.0.

**Fig. S2.** Pseudo-first-order rate constant versus solution pH for the Fenton-like oxidation of OTC with

(a)  $\alpha\text{-MnO}_2$ , (b)  $\beta\text{-MnO}_2$  and (c)  $\gamma\text{-MnO}_2$ . Conditions: [catalysts] = 300 mg/L,  $[\text{H}_2\text{O}_2]$  = 50 mM, [OTC]

= 5 mg/L, pH = 4.0–11.0.

**Fig. S3.** The pH variations versus reaction time in OVs-rich  $\alpha\text{-MnO}_2/\text{H}_2\text{O}_2$  system at initial pH levels

of 4.0 to 11.0.

**Fig. S4.** Zeta potentials of  $\text{MnO}_2$  catalysts as a function of solution pH.

**Fig. S5.** The effect of various anions on OTC degradation in  $\alpha\text{-MnO}_2/\text{H}_2\text{O}_2$  system. Conditions:  $[\text{H}_2\text{O}_2]$

= 50 mM, [OTC] = 5 mg/L,  $[\text{Cl}^-]$  =  $[\text{NO}_3^-]$  =  $[\text{SO}_4^{2-}]$  =  $[\text{PO}_4^{3-}]$  = 1–100 Mm, pH = 7.0.

**Fig. S6.** Solid EPR spectra of  $\alpha\text{-MnO}_2$ ,  $\alpha\text{-MnO}_2\text{-K-2h}$ ,  $\alpha\text{-MnO}_2\text{-K-4h}$  and  $\alpha\text{-MnO}_2\text{-K-6h}$ .

**Fig. S6.** Solid EPR spectra of  $\alpha\text{-MnO}_2$ ,  $\alpha\text{-MnO}_2\text{-K-2h}$ ,  $\alpha\text{-MnO}_2\text{-K-4h}$  and  $\alpha\text{-MnO}_2\text{-K-6h}$ .

**Fig. S7.** XPS spectra of Mn 2p (a) and O 1s (b) of  $\alpha\text{-MnO}_2$  after the reaction.

**Fig. S8.** Degradation of DPBF in sole H<sub>2</sub>O<sub>2</sub> system and adsorption of DPBF by various  $\alpha$ -MnO<sub>2</sub> catalysts. Conditions: [catalysts] = 300 mg/L, [H<sub>2</sub>O<sub>2</sub>] = 50 mM, [DPBF] = 0.05 mmol/L, pH = 11.0.

**Text S1.** Quantitative detection of  $^1\text{O}_2$ .

Since 1,3-diphenylisobenzofuran (DPBF) could react with  $^1\text{O}_2$  in a molar ratio of 1:1, it was applied to quantitatively reflect the production amount of  $^1\text{O}_2$  in the  $\text{H}_2\text{O}_2$  activation system<sup>1</sup>. Typically, 30 mg of different  $\text{K}^+$ -modified  $\alpha\text{-MnO}_2$  catalysts was dispersed in 100 mL of solution with 0.05 mmol/L of DPBF for adsorption–desorption equilibrium. Then, 50 mM of  $\text{H}_2\text{O}_2$  was added to initiate the reaction. The concentration of DPBF was measured by UV-2700 spectrophotometer (Shimadzu Corporation) at 411 nm. In the background experiments (**Fig. S8**), sole  $\text{H}_2\text{O}_2$  system had no degradation ability to DPBF, and the  $\text{K}^+$ -modified  $\alpha\text{-MnO}_2$  catalysts showed negligible adsorption performances for DPBF.

**Text S2.** Density functional theory (DFT) calculation.

We have employed the first-principles<sup>2</sup> to perform all (DFT) calculations within the generalized gradient approximation (GGA) using the Perdew-Burke-Ernzerhof (PBE) formulation<sup>3</sup>. We have chosen the projected augmented wave (PAW) potentials<sup>4</sup> to describe the ionic cores and take valence electrons into account using a plane wave basis set with a kinetic energy cutoff of 400eV. Partial occupancies of the Kohn–Sham orbitals were allowed using the Gaussian smearing method and a width of 0.05 eV. The electronic energy was considered self-consistent when the energy change was smaller than  $10^{-5}$  eV. A geometry optimization was considered convergent when the energy change was smaller than  $0.03 \text{ eV } \text{\AA}^{-1}$ . In our structure, the U correction is used for Mn atoms. The vacuum spacing in a direction perpendicular to the plane of the structure is  $18 \text{ \AA}$  for the  $\text{MnO}_2$  surfaces. The Brillouin zone integration is performed using  $3 \times 3 \times 1$  Monkhorst-Pack k-point sampling for a structure. Finally, the adsorption energies ( $E_{\text{ads}}$ ) were calculated as  $E_{\text{ads}} = E_{\text{ad/sub}} - E_{\text{ad}} - E_{\text{sub}}$ , where  $E_{\text{ad/sub}}$ ,  $E_{\text{ad}}$ , and  $E_{\text{sub}}$  are the total energies of the optimized adsorbate/substrate system, the adsorbate in the structure, and the clean substrate, respectively. The free energy was calculated using the equation:

$$G = E_{\text{ads}} + \text{ZPE} - TS$$

where G,  $E_{\text{ads}}$ , ZPE and TS are the free energy, total energy from DFT calculations, zero point energy and entropic contributions, respectively.

**Table S1.** Parameters of pharmaceutical wastewater.

Parameters	Pharmaceutical wastewater
pH	5.6
COD (mg/L)	66.4
TOC (mg/L)	18.7
UV <sub>254</sub> (cm <sup>-1</sup> )	0.457
Turbidity	9.04
DO (mg/L)	7.38

**Table S2.** Detected emerging organic contaminants in the pharmaceutical wastewater.

Number	Emerging organic contaminants	Concentration ( $\mu\text{g/L}$ )
1	Oxytetracycline	$0.81 \pm 0.10$
2	Lincomycin	$1.73 \pm 0.22$
3	Tetracycline	$1.95 \pm 0.46$
4	Bisphenol A	$3.46 \pm 0.12$
5	Amoxicillin	$4.19 \pm 0.22$
6	Naproxen	$6.67 \pm 1.29$
7	Roxithromycin	$11.09 \pm 0.22$
8	Erythromycin	$18.88 \pm 1.01$
9	Ciprofloxacin	$19.80 \pm 0.10$
10	Paracetamol	$36.49 \pm 3.75$

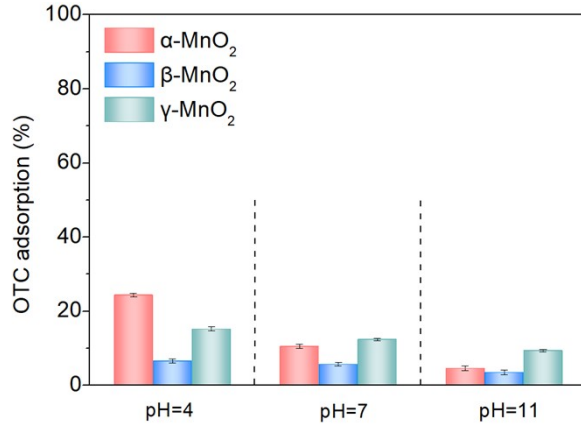


**Fig. S1.** Adsorption of OTC by different MnO<sub>2</sub> catalysts under various pH conditions. Conditions:

[catalysts] = 300 mg/L, [OTC] = 5 mg/L, pH = 4.0–11.0.

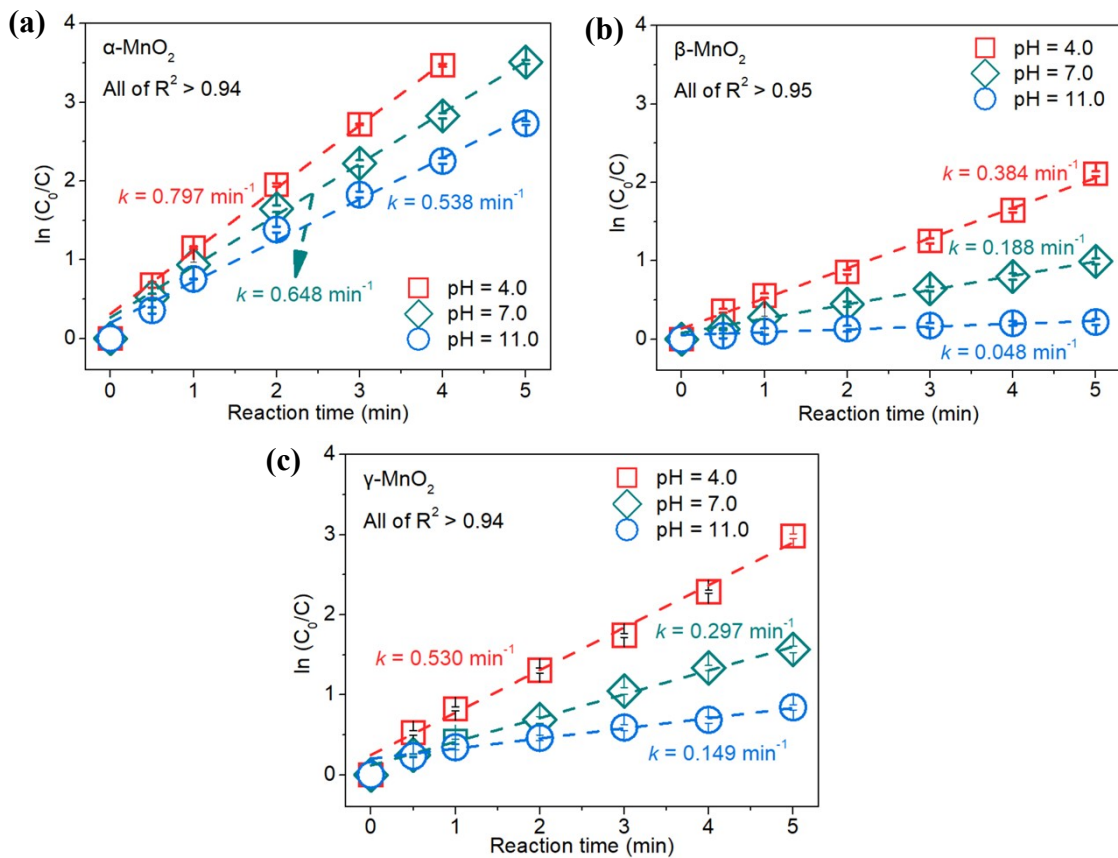


**Fig. S2.** Pseudo-first-order rate constant versus solution pH for the Fenton-like oxidation of OTC with

(a)  $\alpha$ -MnO<sub>2</sub>, (b)  $\beta$ -MnO<sub>2</sub> and (c)  $\gamma$ -MnO<sub>2</sub>. Conditions: [catalysts] = 300 mg/L, [H<sub>2</sub>O<sub>2</sub>] = 50 mM, [OTC]

= 5 mg/L, pH = 4.0–11.0

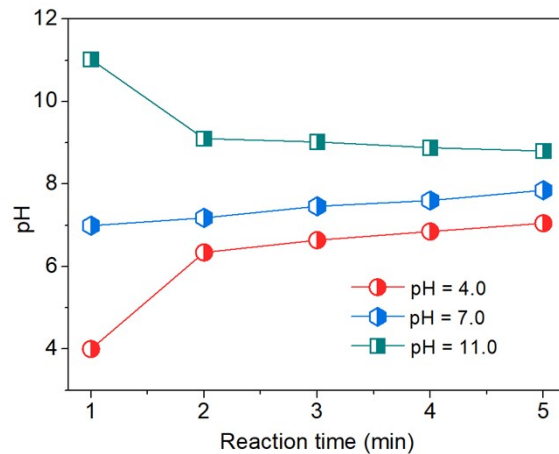


**Fig. S3.** The pH variations versus reaction time in OV<sub>s</sub>-rich  $\alpha$ -MnO<sub>2</sub>/H<sub>2</sub>O<sub>2</sub> system at initial pH levels of 4.0 to 11.0.

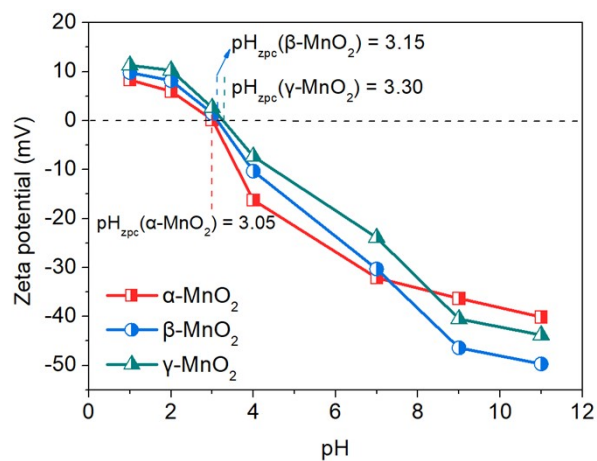


**Fig. S4.** Zeta potentials of MnO<sub>2</sub> catalysts as a function of solution pH.

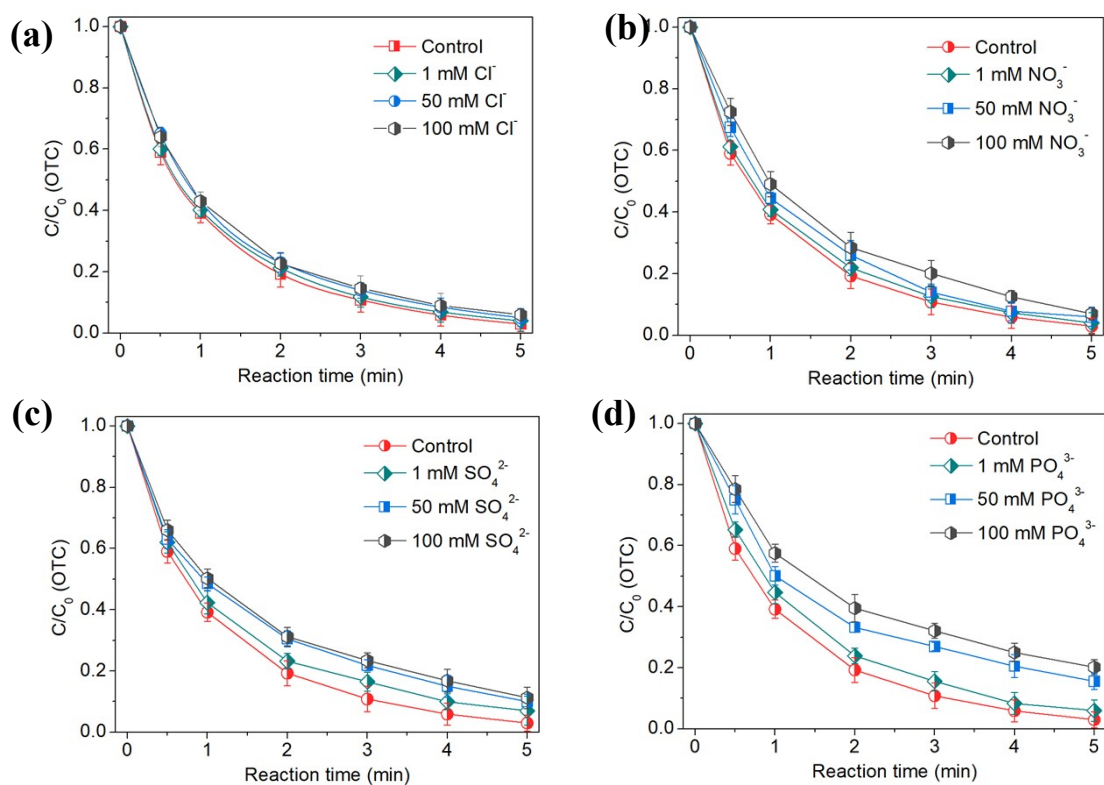


**Fig. S5.** The effect of various anions on OTC degradation in  $\alpha\text{-MnO}_2/\text{H}_2\text{O}_2$  system.

Conditions:  $[\text{H}_2\text{O}_2] = 50 \text{ mM}$ ,  $[\text{OTC}] = 5 \text{ mg/L}$ ,  $[\text{Cl}^-] = [\text{NO}_3^-] = [\text{SO}_4^{2-}] = [\text{PO}_4^{3-}] =$

1–100 Mm,  $\text{pH} = 7.0$ .

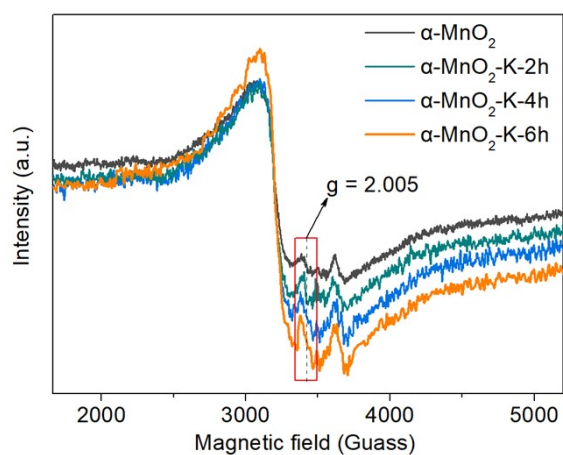


**Fig. S6.** Solid EPR spectra of  $\alpha\text{-MnO}_2$ ,  $\alpha\text{-MnO}_2\text{-K-2h}$ ,  $\alpha\text{-MnO}_2\text{-K-4h}$  and  $\alpha\text{-MnO}_2\text{-K-6h}$ .

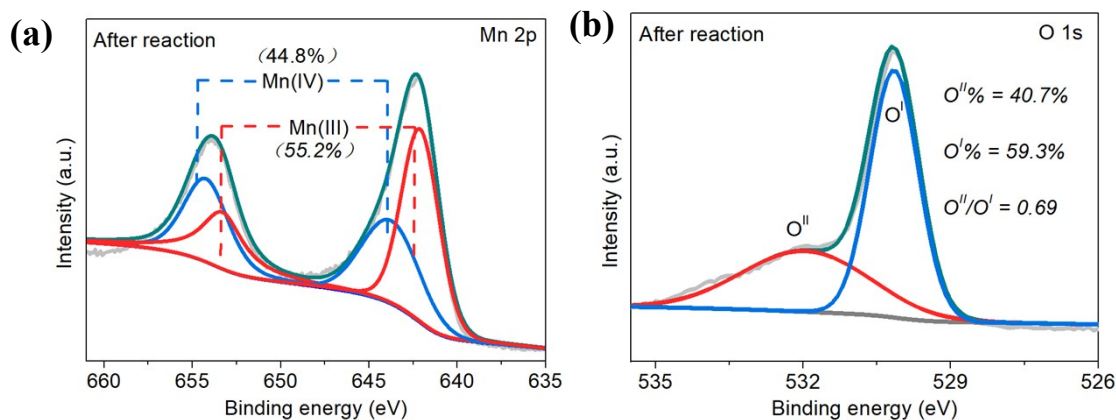


**Fig. S7.** XPS spectra of Mn 2p (a) and O 1s (b) of  $\alpha$ -MnO<sub>2</sub> after the reaction.

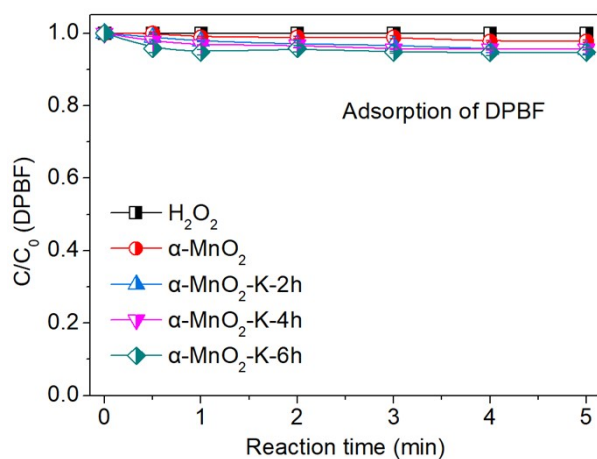


**Fig. S8.** Degradation of DPBF in sole H<sub>2</sub>O<sub>2</sub> system and adsorption of DPBF by various  $\alpha$ -MnO<sub>2</sub> catalysts. Conditions: [catalysts] = 300 mg/L, [H<sub>2</sub>O<sub>2</sub>] = 50 mM, [DPBF] = 0.05 mmol/L, pH = 11.0.

## References

1. S. Liu, C. Lai, X. Zhou, C. Zhang, L. Chen, H. Yan, L. Qin, D. Huang, H. Ye, W. Chen, L. Li, M. Zhang, L. Tang, F. Xu and D. Ma, Peroxydisulfate activation by sulfur-doped ordered mesoporous carbon: Insight into the intrinsic relationship between defects and  $^1\text{O}_2$  generation, *Water. Res.*, 2022, **221**, 118797.
2. G. Kresse and J. Furthmüller, Efficiency of Ab-Initio Total Energy Calculations for Metals and Semiconductors Using a Plane-Wave Basis Set., *Comput. Mater. Sci.*, 1996, **6**, 15-50.
3. J. P. Perdew, K. Burke and M. Ernzerhof, Generalized Gradient Approximation Made Simple, *Phys. Rev. Lett.*, 1996, **77**, 3865–3868.
4. G. Kresse and D. Joubert, From Ultrasoft Pseudopotentials to the Projector Augmented-Wave Method, *Phys. Rev. B*, **59**, 1758-1775.